Physical Communication 29 (2018) 230–244

Contents lists available at ScienceDirect

Physical Communication

journal homepage: www.elsevier.com/locate/phycom

Full length article

Coordinated multipoint in dense heterogeneous networks with overlapping microcell expanded regions and its effect on backhaul links

Jessica Khoriaty, Hassan Artail *, Youssef Nasser

American University of Beirut, Department of Electrical and Computer Engineering, Bliss Street, Beirut, Lebanon

ARTICLE INFO

Article history:
Received 23 September 2017
Received in revised form 28 May 2018
Available online 26 June 2018

Keywords:
CoMP
HetNets
Dense networks
Bias factor
Range expansion
Backhaul

ABSTRACT

One of the goals of Heterogeneous Networks (HetNets) is to offload traffic from the macrocell BS to the microcell base stations (BSs). It has been proposed that in order for the microcell to acquire more users and offload increasing amounts of traffic, its region of coverage must be expanded. This however causes significant cross-tier interference, which can be remedied by utilizing coordinated multipoint (CoMP) within the microcell expanded region (ER). Our methodology considers the effect of overlapping ERs, and proposes the cooperation of concerned microcell BSs with the macrocell BS to further reduce the outage probability and improve throughput. Another important consideration in our analysis is the effect of having non-ideal backhaul on the system's performance. That is, CoMP increases the strain on the backhaul network, since additional data that is proportional to the number of cooperating BSs needs to travel on the backhaul links. Furthermore, the delay should be minimal and less than one subframe duration in order for reported channel state information to remain valid. With this in mind, our proposed system considers the effect of having non-ideal backhaul in a cellular network with CoMP, while taking into account overlaps in the microcell ERs.

1. Introduction

The migration from 3G to 4G systems, brought on by a need to satisfy improved performance requirements, was not achieved by LTE systems, and the enhancements to LTE, under the umbrella of LTE-Advanced, necessitated the introduction of the concept of heterogeneous networks and CoMP to better serve increasing traffic demands [1]. Heterogeneous cellular networks (HetNets) consist of a traditional macrocell tier overlaid with several small cell tiers, each of which is served with a base station (BS) that operates at a lower power and works to offload traffic from the macrocell network. In a homogeneous cellular network, cell association is based on maximum downlink received signal strength [2]. However, in the case of HetNets, this method hinders efficient traffic offloading from the macrocell since the received signal strength from distant macrocell BSs may be stronger than that of closer small cell BSs. Another problem that arises in HetNets is due to the uplink transmission of the macrocell BSs to UEs in the neighborhood of microcells, thus creating interference at those microcells. This issue can be remedied through applying a bias factor [2] at such UEs, which allows for the expansion of the small cell BS coverage area by an amount which is referred to as Expanded Region (ER). This factor is a multiplicative term that serves to increase the received signal strength perceived at the UE, thus causing small cell handover to occur sooner. However, the application of the bias factor increases the level of interference and noise in the ER since the UE is not connected to the cell that provides the strongest signal [3]. Inter cell interference (ICI) coordination is therefore needed to provide better signal quality at the UEs in the ER.

Cooperation between BSs is one of the solutions for ICI, where Coordinated Multipoint (CoMP) is a technique that allows for the transmission and reception of data to a user from a set of different BSs simultaneously. This can make ICI a useful signal in regions that are close to the cell edge and improve signal quality. In joint transmission CoMP, BSs cooperate to transmit the same data to the UE, thus allowing for the mitigation of ICI and the increase of throughput for users at the cell edge [1,4]. Recent works in the literature, as shown in Section 2, benefit from CoMP by allowing cross tier coordination between macrocell and microcell BSs.

Our proposed scheme, unlike previous works on CoMP, considers possible overlaps in the microcell ERs, which are likely to exist when the density of the microcells is high. We use the ER around the microcell as the determining factor for employing the type of CoMP joint transmission. At the perimeter of the microcell

* Corresponding author.
E-mail addresses: jjk11@mail.aub.edu (J. Khoriaty), hartail@aub.edu.lb (H. Artail), yn10@aub.edu.lb (Y. Nasser).

https://doi.org/10.1016/j.phycom.2018.06.008
1874-4907/

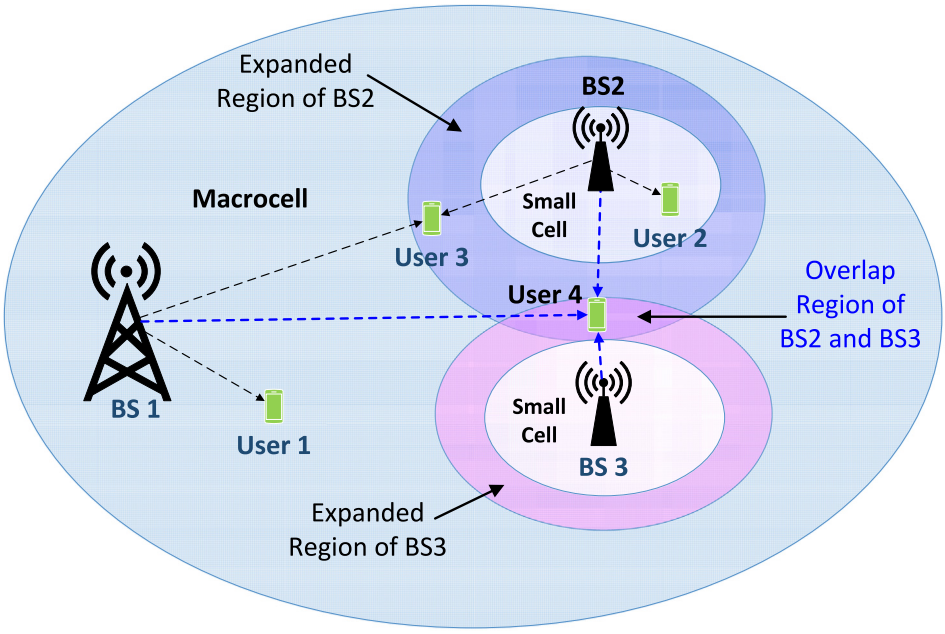

Fig. 1. A network with users in different scenarios (UE4 is served by BS1, BS2, and BS3).

coverage area the power ratio between the macrocell BS (macBS) and the microcell BS (micBS) is 1, whereas at the perimeter of the ER, the same power ratio is equal to a value that is denoted by β. Hence, within the microcell coverage area, the interference from the macBS is no longer significant, and users can be served solely by the micBS. On the other hand, beyond the ER, the power ratio between the macBS and the strongest micBS is greater than β, and the user would be served from the macBS, since interference from the microcell is not significant. Finally, when the power ratio is between 1 and β, CoMP will be employed between the concerned microcell and the macBSs, which is a case that is treated in previous works. However, what has not been addressed in the literature is the case of User 4 in Fig. 1, which lies in the overlap of the two microcell ERs, thus necessitating the three BSs (of the macro and of the two micros) to participate in CoMP.

In addition of addressing the case of UEs that fall within the overlap region of the ERs of multiple microcells, our work also tackles a research challenge that was discussed in [1], namely the effect of having non-ideal backhaul (i.e., an infrastructure with latency and capacity limitations) on CoMP performance. This challenge is not addressed in [5], which we base our work on, although the literature includes work that proposes to reduce the CoMP backhaul burden by selecting a subset of BSs for cooperation, and other work that investigates the effect of non-ideal backhaul on the network. The importance of studying the effect of non-ideal backhaul lies in the fact that CoMP requires an increase in the amount of overhead traveling on the X2 interface, consisting of the data that needs to be transmitted from the serving BS to the other BSs taking part in joint transmission CoMP (JTCoMP), so that multiple BSs can subsequently transmit the same data to the UE simultaneously. In terms of delay, the requirement is that the latency must be less than the duration of one subframe (1 ms), which would ensure the validity of Channel State Information (CSI) against aging channel conditions. In this regards, our work studies the effect of non-ideal backhaul in terms of capacity as well as delay limitations on our JTCoMP scheme.

In this work, we use stochastic geometry to derive performance metrics for location aware CoMP taking into account overlaps in microcell ERs. Relative to the literature (including our previous work in [6]), the contributions of this work can be summarized as follows:

- Deriving performance metrics, most notably outage probabilities, related to location aware CoMP transmission, while accounting for overlaps in microcell Expanded Regions.
- Providing a scalable framework for CoMP by means of a general UE–BS association model, in which an overlap may exist between two or more ERs. This supports scenarios of dense deployment of wireless access devices associated with a large number of microcell base stations, which consequently gives rise to overlaps among microcell ERs.
- Studying the effect of non-ideal backhaul on CoMP in terms of capacity and delay, given the additional load that CoMP adds to the backhaul, especially in terms of data traffic.

In the remainder of this paper, Section 2 discusses the related work, whereas Section 3 presents our scheme and the analysis. Section 4 presents the performance results of our JTCoMP scheme, Section 5 generalizes the number of CoMP cooperating set to more than 3, Section 6 considers the effect of non-ideal backhaul, and finally, Section 7 concludes the paper.

2. Related work

2.1. CoMP in HetNets

CoMP provides several advantages that include mitigating user interference at the cell edge, increasing throughput, and raising average rates. There are two CoMP schemes to be considered. In coordinated scheduling or beamforming, cooperation involves scheduling and control decisions, with data only being transmitted from one BS. In joint transmission CoMP, on the other hand, data is sent simultaneously from several cooperating BSs to be decoded coherently at the receiver. This mitigates the effect of inter-cell interference and increases throughput.

CoMP can be realized through either a centralized or distributed architecture. In the centralized setup, control information and data is collected at a central unit, which then makes decisions on clustering, precoding, and power allocation. On the other hand, a distributed architecture requires CSI to be collected at the serving cell, which then forwards the required information to other BSs within the cooperating cluster. The channel information that is

required to be relayed back to the BSs in CoMP, as part of the CSI, consists of the Channel Quality Indicator, Precoding Matrix Indicator, and Rank Indicator. This CSI is sent as feedback to the BSs, which then cooperate in transmitting data simultaneously to the concerned UEs.

Previous work on CoMP in HetNets mostly focuses on finding analytical models that represent the HetNet architecture which allows for deriving closed form expressions for certain performance metrics. In [7], for example, the authors provide an approach for CoMP in a K-tier HetNet, where performance is analyzed in terms of outage probability. The BSs are distributed according to a spatial Poisson Point Process (PPP), and an ideal backhaul network is assumed. Furthermore, some current interference mitigation solutions depend on coordinating transmissions between BSs through the use of almost blank subframes, reduced power subframes with range expansion bias [8], and spectrum resource partitioning [8]. However, these schemes are disadvantageous since they cause macrocell throughput losses in both the frequency and time domain.

The range expansion bias was proposed to increase the amount of traffic associated with microcells, and is applied to allow UEs to connect to micBSs sooner than if relying on signal to interference and noise ratio (SINR) alone. This is emphasized by the fact that the closer a micBS gets to the macBS, the lower its effective range becomes. This can sometimes mean that a UE could be connected to a BS that is further away instead of a nearby microcell [4]. The bias factor causes the received power from the microcell to be perceived as greater than it actually is, thus allowing for handover to take place sooner. The fundamental drawback of employing this approach, however, is the increase in the amount of interference that such UEs experience due to the fact that they are associated with a BS with relatively lower power.

A recent work that is described in [5] showed that using the bias factor technique alone for increasing the coverage area of a microcell is not sufficient and hence, a CoMP (CoMP) transmission framework between the macBS and the small cell transmitter was suggested. In traditional CoMP, the backhaul network (i.e., X2 Interface) enables BSs to exchange control information and allows them to cooperate in transmitting data to UEs [9] located at a point that is equidistant from three BSs, called a Voronoi vertex [10]. CoMP can be further extended to be applied to heterogeneous networks [1], whereby the advantage of using it between the small cell and macrocell lies in its ability to enhance signal quality without resource partitioning in frequency or time. That is, instead of having the macro BS signals act as interferers in the microcell vicinity, the macBS can now cooperate in transmitting data simultaneously along with the microcell.

A limitation we identified in [5] is that its association criteria do not consider scenarios in which ERs (resulting from applying the bias factor) overlap. Such scenarios could occur in dense deployment of micBSs that may use CoMP to give better coverage to users within the overlap of the ERs of their transmission ranges. Such scenarios may become common place in Internet of Things (IoT) environments, where a large or even huge number of networked devices and machines are packed in a small geographic area, and are correspondingly being served by a large number of micBSs. To address the above limitation, we propose a system in which multiple small cell transmitters perform CoMP with the macBS to strengthen the signal power in areas that include regions of overlap relative to the signal of the macBS. It follows that our proposed work adds a new level of cooperation between cells within the same tier and aims to solve interference problems in those overlapping regions, correspondingly providing a more scalable framework in terms of multiple small cell environments.

2.2. Backhaul considerations

CoMP has a direct effect on backhaul since cooperation among the macrocell and microcell BSs involve sending data through the backhaul for them to subsequently transmit this same data to the UE simultaneously. In the following, we survey the literature that studies the effect of CoMP on the backhaul or how to reduce this effect, and the effect of the backhaul on CoMP.

We start with the work in [11] which aims to reduce the backhaul load due to CoMP by selecting cooperating clusters using a central coordinator instead of full cooperation. It is based on the notion that although inter-cell interference can be removed through full coordination between BSs, this coordination may place a huge strain on the backhaul network. In [12], CoMP is applied only to a subset of users in order to obtain a compromise between the required performance improvement and the backhaul network constraints. The concept of isolation, which is a measure of how close the user is to the cell center, is introduced and then used to group users, where the number of users in each group is determined by taking the backhaul capacity as a constraint. Consequently, those users with weak isolation or close to the cell boundary are the ones that use CoMP. The idea of grouping is also used in [13], which partitions the network into distributed subsystems, with most interferers in the same subsystem.

The work in [14] proposes to reduce the load on backhaul links through the choice of CoMP to be employed. It studies downlink CoMP between two BSs and two users based on different backhaul capacities, and proposes the use of adaptive coordination where the BSs switch between joint transmission and coordinated beamforming based on channel conditions. The effect of varying backhaul topologies on the gains obtained from deploying CoMP is considered in [15], where a set of different scenarios is used to study which BSs are suitable for CoMP joint transmission from the Radio Access Network (RAN) perspective. On the other hand, the work in [16] assigns link failure probabilities to backhaul links as a mean to investigate the impact of unreliable backhaul on network cooperation. The system model assumes that each user collects CSI and sends it to its serving BS.

Work has also been done to provide schemes for network provisioning so that the backhaul would be able to support CoMP. The authors in [17] present a method to estimate the capacity needed for the backhaul network to support joint transmission CoMP, and it was obviously shown that the amount of data exchanged between BSs depends on the size of the cooperating cluster. Similarly, the work in [18] presents an analysis of the backhaul capacity requirements for CoMP based on channel characteristics and cluster size.

In summary, the literature on backhaul in relation to CoMP lacks generality as in the most part it considers ideal backhaul networks, treats one specific type (i.e., wired or wireless), and does not analyze dense deployment scenarios of cooperating micBSs. On the other hand, we analyze the implications of our expanded regions overlap-aware CoMP scheme on the capacity requirements of the backhaul links, and study the resulting overall UE communication delay for all combinations of backhaul network types (wired, wireless with dedicated resources, and wireless with shared resources). Additionally, we account for dense deployments of microcells by virtue of considering the overlaps in the ERs of the microcell BSs.

3. Proposed microcells expanded regions overlap aware design

3.1. Two tier cellular network model

Our model consists of a macrocell tier overlaid with an independent microcell tier. Each tier's BS position is modeled as a two dimensional homogeneous PPP, with spatial intensity λ_1 for the

macrocell and λ_2 for the microcell. BSs belonging to the same tier are assumed to have the same transmit power and fading exponent. Furthermore, the users' positions are distributed according to a homogeneous PPP with spatial intensity λ_u which is greater than λ_1 to increase the probability of each BS having one or more associated UEs [5].

3.2. User association from BS location

The choice of associated BS depends on the ratio of received powers from BSs in the different tiers. The strategy we adopt in this work is to initially consider a maximum association of a UE to be with two microcells in addition to the macrocell, meaning that the UE will be located in the overlap region of the two microcells' ERs. We analyze the performance of CoMP in HetNets while considering this scenario, and then generalize to the overlap region of N microcells ERs.

Hence, we initially consider four modes of operation: macrocell transmission only, microcell transmission only, CoMP between one macrocell and one microcell, and, finally, CoMP between one macrocell and two microcells. These can be abbreviated as the modes: M, P, $2C$, $3C$. In the M mode, the user is associated with a macBS when the ratio between the received power from the macBS to the strongest received power from the micBS is greater than β. This means that the interference due to the micBS is low and coordination would not be necessary. In the P mode, the user is associated with a microcell when the ratio between the received power from the macBS to the strongest received power from the micBS is less than 1. This signifies that the cross tier interference in this zone is low and that cooperation is not necessary as well. The $2C$ mode occurs within the ER of the microcell with the strongest received power at the UE, where the power ratio between the macBS and this micBS is between 1 and β. In this mode, the UE is served by one macro BS and one micro BS since the cross-tier interference is significant within this region. The $3C$ mode occurs when the UE falls in the overlap region of the ERs of two microcells. The consideration of the $3C$ mode (and higher order modes; e.g., $4C$ and $5C$ modes that represent the overlap region of the ERs of three and four microcells, respectively) is one of the two main contributions of this work. Analyzing the effect of the non-ideal backhaul on CoMP is the second main contribution. In $3C$ (and higher order modes), the cooperation of the two microcells (and further microcells) along with the macrocell is rendered necessary due to the fact that they all would cause co-tier interference within the ER.

3.3. BS association

We denote by B the set of BSs that serve a particular user. The following equation (when only considering the overlap between two microcell ERs) gives the possible BS associations to a user.

$$B = \begin{cases} \{x_1\},\ if\ \dfrac{P_1 R_1^{-\alpha_1}}{P_2 R_2^{-\alpha_2}} \geq \beta \\ \{x_2\},\ if\ \dfrac{P_1 R_1^{-\alpha_1}}{P_2 R_2^{-\alpha_2}} \leq 1 \\ \{x_1, x_2\},\ if\ 1 < \dfrac{P_1 R_1^{-\alpha_1}}{P_2 R_2^{-\alpha_2}} < \beta \bigcap \dfrac{P_1 R_1^{-\alpha_1}}{P_3 R_3^{-\alpha_3}} \geq \beta \\ \{x_1, x_2, x_3\},\ if\ 1 < \dfrac{P_1 R_1^{-\alpha_1}}{P_2 R_2^{-\alpha_2}} < \beta \bigcap 1 < \dfrac{P_1 R_1^{-\alpha_1}}{P_3 R_3^{-\alpha_3}} < \beta \end{cases} \quad (1)$$

In (1), $X = \{x_i | i = 1, 2, 3\}$ is the set of indices of the three strongest transmitting BSs to a user, where x_1 is the strongest macBS, x_2 is the strongest micBS, and x_3 is the second strongest micBS. R_i ($i = 1, 2, 3$) is the distance from the user to the corresponding BS, while α is the pathloss exponent. Hence, we have three BSs of interest, one macrocell and two microcells. The terms P_1 and P_2 represent the transmission power which is assumed to be the same for BSs in the same tier, and the threshold β represents the ratio of the power received from the macBS to the strongest micBS (or two strongest) after which 2C (or 3C) cooperation is performed. For the user to be in x_1 and associated with the microcell tier, the ratio of power received from the strongest macrocell to the power received from the strongest microcell should be greater that the threshold β, and likewise, in order for the user to be in the x_2 region and associated solely with a microcell, the ratio of the power between the strongest macrocell and the strongest microcell should be less than 1. Now, for the user to be in the region of x_1 and x_2, i.e., in association with one macrocell and one microcell, there is only one microcell for which the ratio of the power received from the strongest macrocell to that of this microcell lies between 1 and β. This is the microcell expanded region (ER) and can be represented as a ring around the BS coverage area. Finally, for the user to be in the region x_1, x_2, and x_3, i.e., within the overlap region of the ERs of two micBSs, the ratio of the power received from the macrocell to the first microcell should lie between 1 and β, and the same applies to the second microcell. In referring to Fig. 1, we see that the received power by User 4 is within the ERs of both BS2 and BS3, thus the transmission mode 3C is used, where the three BSs cooperate in transmitting to this user. User 3, on the other hand, will be served by BS1 and BS2 since he is only in close proximity to BS2, and is outside the ER of BS3.

The value of β must be chosen so as to create a tradeoff between performance gains and increased backhaul signaling. This is because higher values mean an increase in the amount of coordination being performed in the network as a whole, but at the same time, it would cause more strain on the backhaul network connecting the BSs. An important issue is the ability of a cellular network to be able to support CoMP under non-ideal backhaul conditions. The quality that backhaul links require calls for the handling of data exchange with low communication latency. This challenge, which is not addressed in prior work, is tackled in our work (see Section 5).

3.4. Distance analysis

The probability that a user is in each one of the modes: M, P, $2C$, and $3C$ is denoted by q_M, q_P, q_{2C}, and q_{3C}, respectively. Based on these probabilities, the probability density functions (PDFs) of the distances between a UE and its serving BS are derived. Moreover, the probability of being in each of the four possible regions, as defined in (1), must be obtained. First, based on the analysis in [5], q_M and q_P can be obtained as follows.

$$q_M = 2\pi\lambda_1 \int_{R+} r \exp\left[-\pi(\lambda_1 r^2 + \lambda_2 \left(\frac{\beta P_2}{P_1}\right)^{2/\alpha_2} r^{2\alpha_1/\alpha_2})\right] dr \quad (2)$$

$$q_P = 2\pi\lambda_2 \int_{R+} r \exp\left[-\pi(\lambda_2 r^2 + \lambda_1 \left(\frac{P_1}{P_2}\right)^{2/\alpha_1} r^{2\alpha_2/\alpha_1})\right] dr \quad (3)$$

The probability q_{3C} can be derived by considering that the UE is associated with three BSs in case it is simultaneously in the ERs of two microcell BSs. Hence, the probability of the UE being in the ER of the microcell with the second strongest received power must also be obtained. This is equivalent to the probability of having the power ratio between the strongest microcell BS and the second strongest microcell BS be less than β. This means that the second

microcell BS can be used for CoMP as well since the two microcells are close together.

$$q_{3C} = (1 - q_P)P\left(\frac{P_1R_1^{-\alpha_1}}{P_2R_2^{-\alpha_2}} < \beta\right)P\left(\frac{P_1R_1^{-\alpha_1}}{P_3R_3^{-\alpha_3}} < \beta\right) \tag{4}$$

The multiplication by the factor $(1 - q_P)$ is to exclude the common region between the macro BS and each of the micro BSs that is not common with the other micro BSs, which corresponds to $\frac{P_1R_1^{-\alpha_1}}{P_2R_2^{-\alpha_2}} \leq 1$ and $\frac{P_1R_1^{-\alpha_1}}{P_3R_3^{-\alpha_3}} \leq 1$. Eq. (4) can be simplified, as illustrated in (5), if we consider that the microcell BSs have the same transmission power, have the same pathloss exponent, and on average are equidistant from the UE.

$$q_{3C} = (1 - q_P)P\left(\frac{P_1R_1^{-\alpha_1}}{P_2R_2^{-\alpha_2}} < \beta\right)^2 \tag{5}$$

where

$$P\left(\frac{P_1R_1^{-\alpha_1}}{P_2R_2^{-\alpha_2}} < \beta\right) = 2\pi\lambda_2\int_{R+} r\exp\left[-\pi(\lambda_2 r^2 + \lambda_1\left(\frac{P_1}{\beta P_2}\right)^{2/\alpha_1} r^{2\alpha_2/\alpha_1})\right]dr. \tag{6}$$

We note that the simplification in (5) does not mean that R_3 is independent of R_2, but it implicitly states that, to be in the intersection of the three BSs, the distance between the UE and each of the mircoBSs is on average the same when considering all the scenarios in which the UE is in the overlap region.

The remaining case, namely the probability of being in mode q_{2C}, can be inferred as follows.

$$q_{2C} = 1 - q_M - q_P - q_{3C} \tag{7}$$

Next, the PDFs of the distances between a UE and its serving BSs are obtained based on [5].

$$f_{R_M}(r) = \frac{2\pi\lambda_1}{q_M} r\exp\left[-\pi\left(\lambda_1 r^2 + \lambda_2\left(\frac{\beta P_2}{P_1}\right)^{2/\alpha_2} r^{2\alpha_1/\alpha_2}\right)\right] \tag{8}$$

$$f_{R_P}(r) = \frac{2\pi\lambda_2}{q_P} r\exp\left[-\pi\left(\lambda_2 r^2 + \lambda_1\left(\frac{P_1}{P_2}\right)^{2/\alpha_1} r^{2\alpha_2/\alpha_1}\right)\right] \tag{9}$$

In order to obtain the PDF of the mode *3C*, we need to consider the probability that there are no BSs in a disk of radius r to the reference point in a PPP. We start with the general CDF formulation of the null probability in a PPP, given in (10) below.

$$P[\text{no BSs in a disk of radius } r] = \exp\left[-\pi\lambda r^2\right] \tag{10}$$

Then the PDF of having at least one BS inside the disk is

$$f_r'(r) = \frac{d}{dr}\left(1 - \exp[-\pi\lambda r^2]\right) = 2\pi\lambda r\exp\left[-\pi\lambda r^2\right]. \tag{11}$$

Following a similar formulation, along with the work of [5], the PDF of the *3C* mode follows.

$$f_{R_{3C}}(r) = \frac{d^3}{dr_1 dr_2 dr_3} \times \left(1 - P\left[R_1 > r_1, R_2 > r_2, R_3 > r_3 | B = \{x_1, x_2, x_3\}\right]\right) \tag{12}$$

$$f_{R_{3C}}(r) = \frac{8\pi^3\lambda_1\lambda_2^2}{q_{3C}} r_1 r_2 r_3\exp\left[-\pi\left(\lambda_2\left(r_2^2 + r_3^2\right) + \lambda_1 r_1^2\right)\right] \tag{13}$$

Similarly, the PDF of the mode *2C* can be obtained as

$$f_{R_{2C}}(r) = \frac{4\pi^2\lambda_1\lambda_2}{q_{2C}} r_1 r_2\exp\left[-\pi\left(\lambda_2 r_2^2 + \lambda_1 r_1^2\right)\right]. \tag{14}$$

The PDF expressions in (13) and (14) are used to get the ones for the outage probabilities in the next section.

3.5. Outage probability analysis

In this section an expression for the outage probability is obtained based on certain SINR analysis. In this paper, we assume interfering signals to be independent. To start with, the received signal power at a user can be expressed as follows.

$$\sum_{x_i \in B} \frac{\sqrt{P}h_w}{\|x_i\|^{\frac{\alpha}{2}}} W + \sum_{x_i \in B^C} \frac{\sqrt{P}g_y}{\|x_i\|^{\frac{\alpha}{2}}} Y + Z \tag{15}$$

where the first sum represents the useful signal, while the second sum represents the interference component. The term B^C denotes the complement of the set B, and represents the BSs that are interferers at the UE, and which are not participating in the transmission to the concerned UE. The terms h_w and g_y are the small scale fading coefficients that are assumed to be Rayleigh distributed, leading to a power distribution with exponential amplitude and uniform phase. The variable α is the pathloss exponent, while W and Y are random variables that represent the data sequences that are transmitted from the serving and interfering BSs. Finally, Z is the Additive White Gaussian noise (AWGN), and we assume a channel with no CSI at the receiver.

The outage probability is the probability that the received SINR is lower than a certain threshold τ. The equation below defines the outage probability for different modes of operation i. A is the region of integration over $\{r_1, r_2, r_3\}$ which is the distance between a UE and its serving BS. This value is different for each mode of operation as it indicates the locations in which a UE is in order to be associated with each mode.

$$O_i = 1 - \int_A P\left[SINR\left(B\right) > \tau\right] f_{R_i}(r)dr \tag{16}$$

For the different modes, we have corresponding outage probabilities, defined as O_M, O_P, O_{2C}, and O_{3C}. For instance, the outage probability O_M can be defined as the probability that the SINR at a UE operating in the M mode is lower than τ. Assuming that BSs are sending signals that are not coherently aligned, the outage probability can be derived for each mode as follows.

$$O_M = 1 - \int_A P\left[\frac{\left|\sqrt{P_1}h_1\left\|x_1\right\|^{\frac{-\alpha_1}{2}}\right|^2}{\sum_{x_i \neq x_1} P_i|g_i|^2\left\|x_i\right\|^{-\alpha_i} + Z} > \tau\right] f_{R_M}(r)dr \tag{17}$$

$$O_P = 1 - \int_A P\left[\frac{\left|\sqrt{P_2}h_2\left\|x_2\right\|^{\frac{-\alpha_2}{2}}\right|^2}{\sum_{x_i \neq x_2} P_i|g_i|^2\left\|x_i\right\|^{-\alpha_i} + Z} > \tau\right] f_{R_P}(r)dr \tag{18}$$

$$O_{3C} = 1 - \int_A P \times \left[\frac{\left|\left|\sqrt{P_1}h_1\left\|x_1\right\|^{\frac{-\alpha_1}{2}}\right| + \left|\sqrt{P_2}h_2\left\|x_2\right\|^{\frac{-\alpha_2}{2}}\right| + \left|\sqrt{P_2}h_3\left\|x_3\right\|^{\frac{-\alpha_2}{2}}\right|\right|^2}{\sum_{x_i \neq x_1, x_2, x_3} P_i|g_i|^2\left\|x_i\right\|^{-\alpha_i} + Z} > \tau\right] f_{R_{3C}}(r)dr \tag{19}$$

$$O_{2C} = 1 - \int_A P\left[\frac{\left|\left|\sqrt{P_1}h_1\left\|x_1\right\|^{\frac{-\alpha_1}{2}}\right| + \left|\sqrt{P_2}h_2\left\|x_2\right\|^{\frac{-\alpha_2}{2}}\right|\right|^2}{\sum_{x_i\neq x_1,x_2} P_i|g_i|^2\left\|x_i\right\|^{-\alpha_i} + Z} > \tau\right] \times f_{R_{2C}}(r)dr \tag{20}$$

Since the different modes are mutually exclusive, the overall outage probability can then be

$$O = q_M O_M + q_P O_P + q_{2C} O_{2C} + q_{3C} O_{3C}. \tag{21}$$

The outage probabilities for users in each mode are then derived starting from the SINR expression as follows. First, assuming that h and g are i.i.d. with a complex Gaussian distribution CN (0,1), the outage probabilities O_M and O_P are directly derived from [5] (Appendix B):

$$O_M = 1 - \int_{R+} \exp\left[\frac{-\tau\sigma_z^2}{P_1 r^{-\alpha_1}}\right]\prod_{j=1}^{2} L_{l_j}\left(\frac{\tau r^{\alpha_1}}{P_1}\right) f_{R_M}(r)dr \tag{22}$$

$$O_P = 1 - \int_{R+} \exp\left[\frac{-\tau\sigma_z^2}{P_2 r^{-\alpha_2}}\right]\prod_{j=1}^{2} L_{l_j}\left(\frac{\tau r^{\alpha_2}}{P_2}\right) f_{R_P}(r)dr \tag{23}$$

The above is true because the association of a user with a macro BS or a micro BS is not affected by considering users in the overlap ERs differently than those in non-overlapped ERs.

Next, the derivation of O_{3C} starts by the probability expression in (19) as follows.

$$P\left[\frac{\left|\left|\sqrt{P_1}h_1\left\|x_1\right\|^{\frac{-\alpha_1}{2}}\right| + \left|\sqrt{P_2}h_2\left\|x_2\right\|^{\frac{-\alpha_2}{2}}\right| + \left|\sqrt{P_3}h_3\left\|x_3\right\|^{\frac{-\alpha_3}{2}}\right|\right|^2}{\sum_{x_i\neq x_1,x_2,x_3} P_i|g_i|^2\left\|x_i\right\|^{-\alpha_i} + Z} > \tau\right] =$$
$$P\left[\frac{\left|\left|\sqrt{P_1}h_1\left\|x_1\right\|^{\frac{-\alpha_1}{2}}\right| + \left|\sqrt{P_2}h_2\left\|x_2\right\|^{\frac{-\alpha_2}{2}}\right| + \left|\sqrt{P_3}h_3\left\|x_3\right\|^{\frac{-\alpha_3}{2}}\right|\right|^2}{\sum_{i\neq 1,2,3} I_i + Z} > \tau\right] =$$
$$P\left[\left|\left|\sqrt{P_1}h_1\left\|x_1\right\|^{\frac{-\alpha_1}{2}}\right| + \left|\sqrt{P_2}h_2\left\|x_2\right\|^{\frac{-\alpha_2}{2}}\right| + \left|\sqrt{P_3}h_3\left\|x_3\right\|^{\frac{-\alpha_3}{2}}\right|\right|^2 > \tau\left(\sum_{i\neq 1,2,3} I_i + Z\right)\right] \tag{24}$$

In the above, $I_i = P_i|g_i|^2\left\|x_i\right\|^{-\alpha_i}$. We consider again that the coefficients h_i are independent and identically distributed, i.i.d., with a complex Gaussian distribution, hence their powers have an exponential distribution. To write the pdf in (24), it is very important to derive the pdf of the LHS of the expression. In this respect, we can write:

$$\left|\left|\sqrt{P_1}h_1\left\|x_1\right\|^{\frac{-\alpha_1}{2}}\right| + \left|\sqrt{P_2}h_2\left\|x_2\right\|^{\frac{-\alpha_2}{2}}\right| + \left|\sqrt{P_2}h_3\left\|x_3\right\|^{\frac{-\alpha_2}{2}}\right|\right|^2 \sim Exp\left(\frac{1}{\sum_{i=1}^{3}\left(\sqrt{P_i}\left\|x_i\right\|^{\frac{-\alpha_i}{2}}\right)^2}\right) \tag{25}$$

Then, (24) yields:

$$\int_{\tau\left(\sum_{j\neq 1,2,3} I_j + Z\right)}^{\infty} \exp\left(\frac{1}{\sum_{i=1}^{3}\sqrt{P_i}\left\|x_i\right\|^{\frac{-\alpha_i}{2}}}\right) dx_i \tag{26}$$

Next, it is required to integrate this probability in terms of interference. Using, the Probability Generating Functional (PGFL), the probability terms becomes:

$$P[SINR > \tau] = Exp\left(\frac{-\tau\sigma_z^2}{\sum_{i=1}^{3}\left(\sqrt{P_i}\left\|x_i\right\|^{\frac{-\alpha_i}{2}}\right)^2}\right) \times \prod_{j=1}^{2} L_{l_j}\left(\frac{\tau}{\sum_{i=1}^{3}\left(\sqrt{P_i}\left\|x_i\right\|^{\frac{-\alpha_i}{2}}\right)^2}\right)$$

Next, the expressions for O_{3C} and O_{2C} follow.

$$O_{3C} = 1 - \int_{3C} \exp\left[\frac{-\tau\sigma_z^2}{P_1 r_1^{-\alpha_1} + P_2 r_2^{-\alpha_2} + P_2 r_3^{-\alpha_2}}\right] \times \prod_{j=1}^{2} L_{l_j}^*\left(\frac{\tau}{P_1 r_1^{-\alpha_1} + P_2 r_2^{-\alpha_2} + P_2 r_3^{-\alpha_2}}\right) f_{R_{3C}}(r)dr \tag{27}$$

$$O_{2C} = 1 - \int_{2C} \exp\left[\frac{-\tau\sigma_z^2}{P_1 r_1^{-\alpha_1} + P_2 r_2^{-\alpha_2}}\right] \times \prod_{j=1}^{2} L_{l_j}^*\left(\frac{\tau}{P_1 r_1^{-\alpha_1} + P_2 r_2^{-\alpha_2}}\right) f_{R_{2C}}(r)dr \tag{28}$$

where σ_z is the variance of the AWGN, and L_{li}^* is defined as in [5] and shown below.

$$L_{l_j}\left(\frac{\tau r^{\alpha_i}}{P_i}\right) = \exp\left[-2\pi\lambda_j\left(\tau\frac{P_j}{P_i}\right)^{\frac{2}{\alpha_j}} r^{\frac{2\alpha_i}{\alpha_j}} F\left(\left(\frac{a_{ij}}{\tau}\right)^{\frac{1}{\alpha_j}}, \alpha_j\right)\right] \tag{29}$$

$$L_{l_j}^*(s) = \exp\left[-2\pi\lambda_j\left(sP_j\right)^{\frac{2}{\alpha_j}} F\left(\left(\frac{1}{sP_j}\right)^{\frac{1}{\alpha_j}}, \alpha_j\right)\right] \tag{30}$$

where a_{ij} is equal to β when $i = 1$ and $j = 2$ and is equal to 1 otherwise, while $F(y, \alpha)$ is defined as

$$F(y, \alpha) = \int_y^{\infty} \frac{u}{1 + u^{\alpha}} du. \tag{31}$$

Obtaining the value of O_{2C} involves integrating the expression in (28) over the region 2C, which is defined by the limits of the following two variables.

$$r_1 \geq 0; \quad \left(\frac{P_2}{P_1}\right)^{\frac{1}{\alpha_2}} r_1^{\frac{\alpha_1}{\alpha_2}} < r_2 < \left(\frac{\beta P_2}{P_1}\right)^{\frac{1}{\alpha_2}} r_1^{\frac{\alpha_1}{\alpha_2}} \tag{32}$$

The limits of r_2, which is the distance between the UE and the strongest transmitting microcell, are obtained from the ring conditions, resulting from the microcell ER. Furthermore, obtaining the value of O_{3C} involves integrating the expression in (27) over the region 3C, defined by the limits of the following three variables.

$$r_1 \geq 0; \quad \left(\frac{P_2}{P_1}\right)^{\frac{1}{\alpha_2}} r_1^{\frac{\alpha_1}{\alpha_2}} < r_2, \ r_3 < \left(\frac{\beta P_2}{P_1}\right)^{\frac{1}{\alpha_2}} r_1^{\frac{\alpha_1}{\alpha_2}} \tag{33}$$

As can be seen in the limits above, r_2 is limited to be within the microcell ER. The same applies to r_3 in the case of O_{3C}, where both r_2 and r_3 are jointly bounded by the same limits.

4. Experimental results

In this section, we simulate the effect of considering overlaps in the microcell ERs on the average performance of the entire

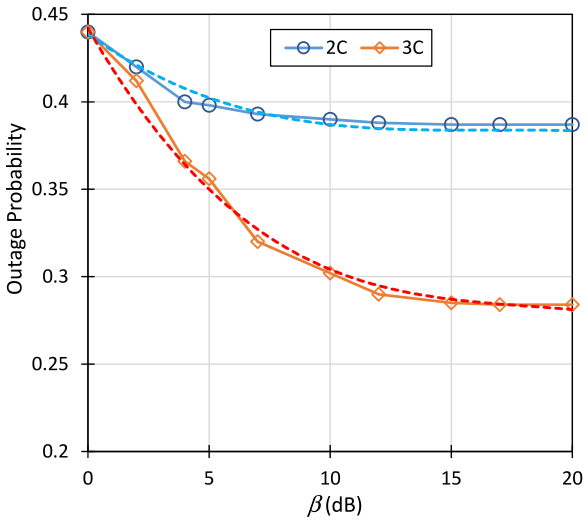

Fig. 2. Outage probability vs. β, with numerical (solid) and theoretical (dashed) results.

network. Further analysis will also be done to show the gains obtained for users that lie within the microcell ER. These results are then compared with having no *3C* mode (systems in the literature), which means we only have cooperation between one macrocell and one microcell within the ER. This mode will be referred to as *2C* only.

The Monte Carlo simulation was done for an area of 10 km$\times$10 km, and consistent with the literature, the Tx powers of the macro BSs and micro BSs were set to be 37 dBm and 20 dBm respectively, while the variance of the AWGN channel was set to -104 dBm. Furthermore, the macrocell tier has a BS intensity $\lambda_1 = (\pi \times 500^2)^{-1}$ nodes/m^2, the microcell tier BS intensity $\lambda_2 = 10\lambda_1$, while the intensity of UEs is $\lambda_u = 20\lambda_1$. The BSs and UEs are simulated as independent Poisson Point Processes, and the analysis is done based on the resulting distance between the UEs and each BS. Finally, the pathloss exponents, α_1 and α_2, were set to 4, while the SINR threshold was set to 0 dB.

We validate the theoretical results from the analysis performed in the previous section, against the experimental ones. We first show in Fig. 2 the average network outage probability, while varying the value of β from 0 to 20 dBs, for both the 2C case (for reference) and for 3C.

We observe in Fig. 2 how the theoretical results match with the experimental ones very closely, thus proving the validity of the theoretical model that we developed. Therefore, all further results will be based on the experimental simulations. We also note that for β values above 10 dBs, the average gain in the *overall network* (i.e., drop in outage probability) stabilizes at 0.1.

Next, we illustrate how the outage probability varies when varying the intensity of microcells and varying the average distance between the UE and the serving BSs. In this experiment, a value of 8 dBs was considered for β, and the ratio $\lambda_2/\ \lambda_1$ was increased from 1 to 20 while fixing λ_u/λ_2 to 2. The results indicate that as the microcell BS intensity increases, we see more benefit in employing *3C* CoMP, as the difference between the overall outage probabilities increases for lower average distance (i.e., denser deployments of microcells). This is expected since as the number of microcells with respect to macrocells increases, more overlap among the expanded regions exists.

In both graphs of Fig. 3, we plot the results of the Monte Carlo simulations, with solid lines and markers, and the theoretical results, using dashed lines. On average, the simulation results are very close to the theoretical ones, thus proving the validity of our model and its derivations. The left graph of Fig. 3 shows how the outage probability starts to increase after a certain point as the number of microcells increases further. This can be explained by the fact that as the microcells are operating at a fixed power (consistent with the literature) within a fixed area, the interference level among them increases. Decreasing the microcell BS transmit power leads to a shift in the point at which outage probability starts to increase, until we no longer have an increase in outage probability for lower transmit powers, like at 10 dBm. This shows that an unbounded increase in the microcell tier density would not be beneficial if the microcells are to continue to operate at the same power level.

In the first part of the next experiment, the value of β was set to 10 dB (consistent with the outcome from Fig. 2), while the SINR threshold τ was varied between -10 and 20 dB. It helps to remind that τ is a value below which the network experiences outage, and that it is a design parameter selected to satisfy certain quality-of-service requirements of users. On the other hand, β represents the ratio between the powers received from the serving macro BS and the strongest micro BS, respectively.

The left graph in Fig. 4 demonstrates the percent gain in *network-wide* outage probability that is obtained by considering a CoMP scheme that accounts for overlap among microcell ERs. The plot shows performance improvement of up to 6.5% when compared to not considering overlap regions, which decays as the SINR threshold increases. This improvement appears to be relatively low, but we emphasize that this is the outage probability *over the entire network* covering UEs that are served by the macrocell BS alone (*M* mode), by a microcell BS alone (*P* mode), by the macrocell BS plus a microcell BS (2*C* mode), as well as by the microcell BS plus two microcell BSs (3*C* mode). The right graph of Fig. 4 shows the improvement (relative to not considering ERs, i.e., the scheme in [5]) in network wide outage probability versus β, which was varied from 0 to 20 dB, while fixing the SINR threshold at 0 dB. The explanation for the improvement is that as β increases, more users will be in the microcell ER, and in the overlap region, leading to a better overall performance. We also note that, as seen in Fig. 4, the improvement is computed from both the numerical results and from the analytical results, where, as in the case of Fig. 3, there is general consistency between the two results.

Finally, Fig. 5 illustrates the benefits in terms of outage probability for users *within* the microcell ER, when varying the value of the bias factor β. Again, and as defined in Section 1, β is a multiplicative term that serves to increase the received signal strength perceived at the UE. The figure shows how the outage probability decreases for users where there is cooperation among three BSs. Furthermore, we highlight the improvement through the right graph by displaying the percentage improvement in outage probability (over not having the 3C mode) for users in the overlap region, which can reach 43%.

5. Extending from 3*C* mode to *NC* mode

This section shows how to extend our analysis to the general case in which there are *N* microcell BSs with overlapping expanded regions. This is done in order to provide a more general formulation of our framework, and further demonstrate the benefits received from having co-tier along with cross tier cooperation. We basically follow the same approach as in Section 3 to derive the outage probabilities, but we leave out much of the derivation details due to space restrictions and since the formulas in the most part can be derived by extension. Moreover, in the analysis below, the variable *N* denotes the number of cooperating base stations in each scenario within the network. That is, when there exists an overlap among 5 microcell base stations' expanded regions, the value of *N* will be 6 (to include the macrocell BS), whereas for another region in the

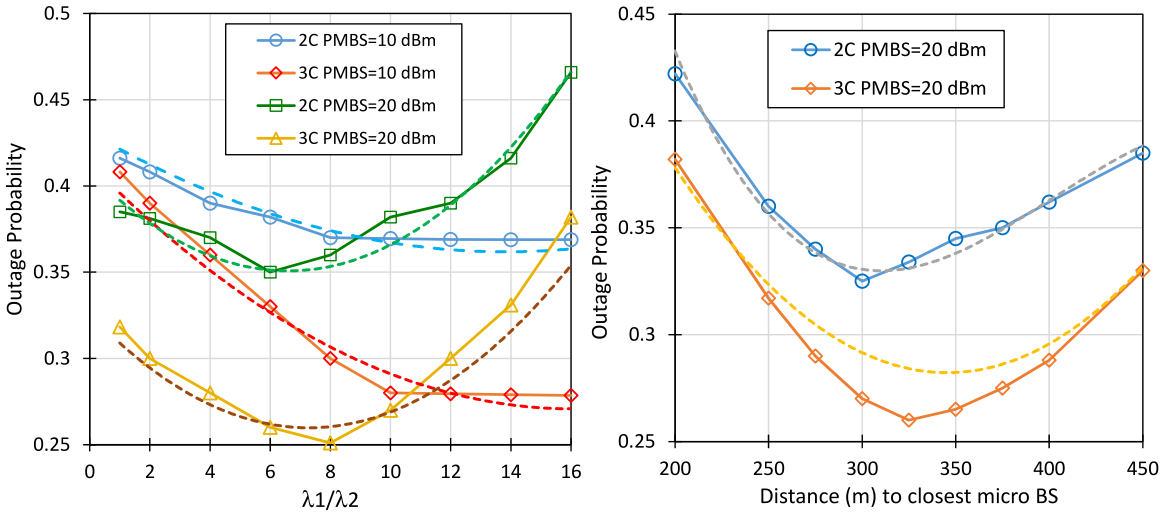

Fig. 3. Outage probability vs. λ_2/λ_1(left), and distance to closest 3 BSs (right). The solid lines are numerical results, while the dashed lines are theoretical results. The term PMBS stands for power of micro base station.

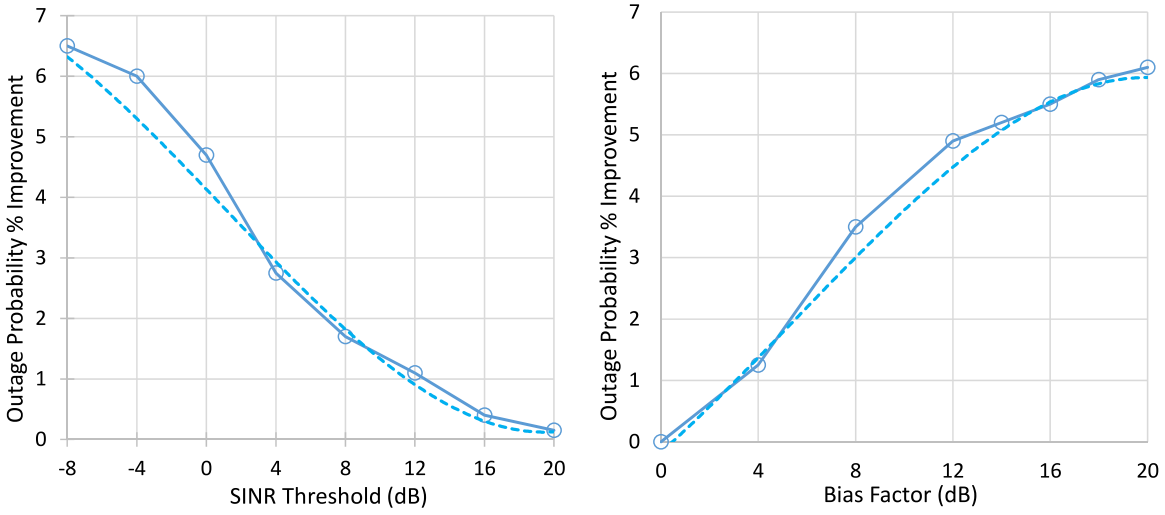

Fig. 4. Network-wide outage probability improvement of 3C relative to 2C.

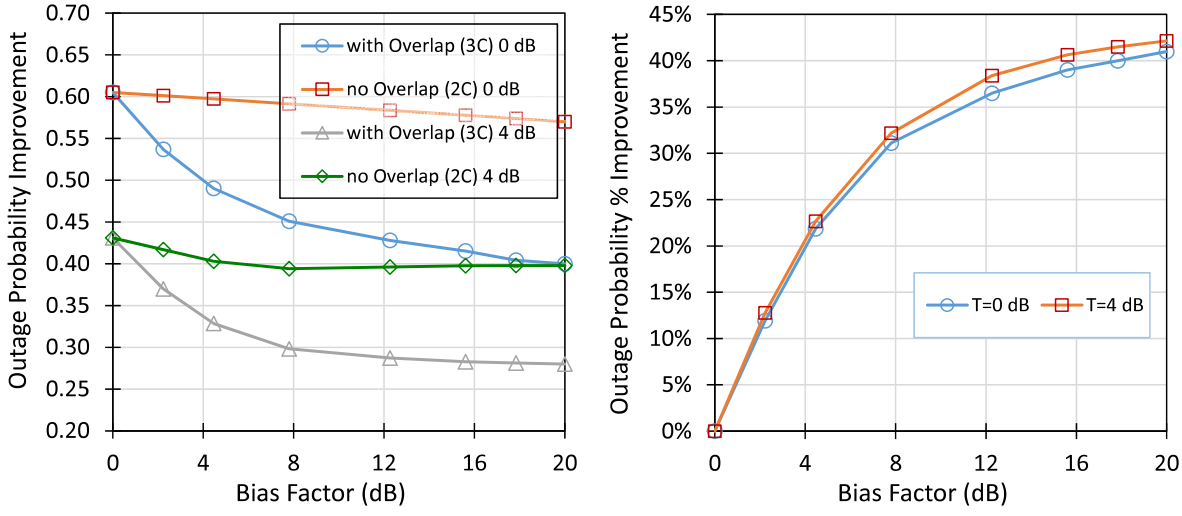

Fig. 5. Outage probability within the ER (left) and percent improvement (right).

network where there is an overlap among the ERs of 3 microcell BSs, the value of N will be 4, and so on. The first step is to extend (1) and define the different modes of operations. This is shown in (34).

$$B = \begin{cases} \{x_1\},\ if\ \dfrac{P_1R_1^{-\alpha_1}}{P_2R_2^{-\alpha_2}} \geq \beta \\ \{x_2\},\ if\ \dfrac{P_1R_1^{-\alpha_1}}{P_2R_2^{-\alpha_2}} \leq 1 \\ \{x_1, x_2\},\ if\ 1 < \dfrac{P_1R_1^{-\alpha_1}}{P_2R_2^{-\alpha_2}} < \beta \bigcap_{l=3}^{N} \dfrac{P_1R_1^{-\alpha_1}}{P_lR_l^{-\alpha_i}} \geq \beta \\ \cdots \\ \{X - x_j - x_k\},\ if\ \exists j,k \left| \bigcap_{i=1,i\neq j,i\neq k}^{N} 1 < \dfrac{P_1R_1^{-\alpha_1}}{P_iR_i^{-\alpha_i}} < \beta \right. \\ \qquad \bigcap_{l=j,k} \dfrac{P_1R_1^{-\alpha_1}}{P_lR_l^{-\alpha_i}} \geq \beta \\ \{X - x_j\},\ if\ \exists j \left| \bigcap_{i=1,i\neq j}^{N} 1 < \dfrac{P_1R_1^{-\alpha_1}}{P_iR_i^{-\alpha_i}} < \beta \bigcap \dfrac{P_1R_1^{-\alpha_1}}{P_jR_j^{-\alpha_j}} \geq \beta \right. \\ \{x_1, x_2, \ldots, x_N\},\ if \bigcap_{i=1}^{N} 1 < \dfrac{P_1R_1^{-\alpha_1}}{P_iR_i^{-\alpha_i}} < \beta \end{cases} \quad (34)$$

Next, in the following, we define the probabilities for Modes NC, where $N \geq 3$.

$$q_{NC} = (1 - q_P)P\left(\frac{P_1R_1^{-\alpha_1}}{P_2R_2^{-\alpha_2}} < \beta\right)^N \quad (35)$$

$$\cdots$$

$$\forall K \in \{1, 2, \ldots, N-4\} : q_{(N-K)C} = (1 - q_P)P\left(\frac{P_1R_1^{-\alpha_1}}{P_2R_2^{-\alpha_2}} < \beta\right)^{N-K} - \sum_{k=1}^{K} q_{(N+1-k)C} \quad (36)$$

where the probabilities q_P and $P\left(\frac{P_1R_1^{-\alpha_1}}{P_2R_2^{-\alpha_2}} < \beta\right)$ were defined earlier in (3) and (6).

Next, the PDFs of the distances between the UE and its serving BSs can be obtained. For space consideration, we only show in the following the PDF of the distance to the Nth serving BS.

$$f_{R_{NC}}(r) = \frac{2^N\pi^N\lambda_1\lambda_2^{N-1}}{q_{NC}} \prod_{i=1}^{N} r_i \exp[-\pi(\lambda_2 \sum_{j=2}^{N} r_j^2 + \lambda_1 r_1^2)] \quad (37)$$

Finally, the corresponding outage probabilities in any mode can be obtained. The outage probability for the user in NC mode ($N \geq 3$) is given by:

$$O_{NC} = 1 - \int_A P\left[\frac{\left|\left|\sqrt{P_1}h_1 \|x_1\|^{\frac{-\alpha_1}{2}}\right| + \sum_{i=2}^{N}\left|\sqrt{P_2}h_i \|x_i\|^{\frac{-\alpha_i}{2}}\right|\right|^2}{\sum_{x_i\neq x_1,x_2,x_3} P_i|g_i|^2 \|x_i\|^{-\alpha_i} + Z} > \tau\right] \times f_{R_{NC}}(r)dr \quad (38)$$

Finally, we simulate the effect of having N overlapping microcell ERs using the same simulation parameters discussed previously, but allowing for the cooperation of N microcell BSs. The

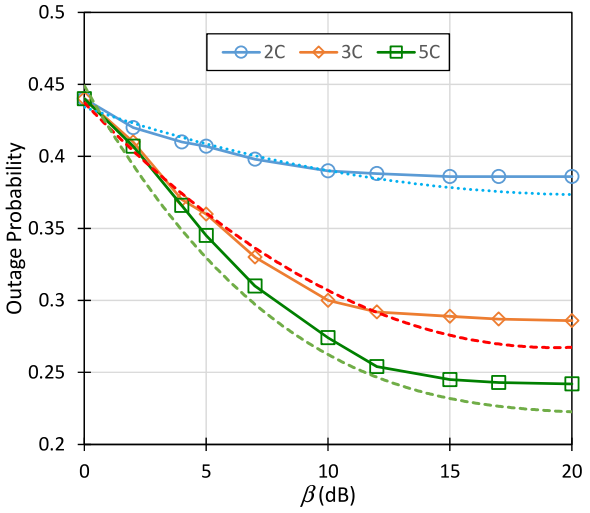

Fig. 6. Outage probability for 2C, 3C, and 5C in entire network.

outage probability results of Fig. 6 (corresponding to (38)) account for cooperation of the microcell BSs in all overlap regions. More specifically, in the tested scenario, the value of N was 5, and so, for UEs in the overlap regions of 5 ERs, all 5 concerned microcell BSs along with the macrocell BS cooperated to transmit to the UEs, whereas in the overlap regions involving 3 ERs, for example, only the concerned 3 microcell BSs cooperated with the macrocell BS to transmit to those UEs. The figure illustrates the average benefit when computed across the whole network and considering all overlap regions. It can be seen that the results of N ($N = 5$) cooperating microcell BSs follow the same trend but provide improvement in outage probability as compared to 3C only. As illustrated, this improvement (relative to 2C) is expected to be higher with the increase of N. For instance, an additional improvement of about 5% is obtained when the system moves from 3C to 5C with β values greater than 10 dBs. Given the improvement of more than 10% when moving from 2C to 3C, we can expect for this improvement to grow at progressively smaller rates as N is increased. Moreover, involving more BSs in CoMP comes at a cost, most notably in terms of consuming backhaul link resources, a subject that we tackle in the next section. Finally, it is worth commenting on the agreement between the analytical results (dashed curves) and the numerical results, although we see minor deviations at high β values.

6. Backhaul considerations

To study the implications of our general CoMP scheme on the capacity and delay aspects of the network backhaul, we outline some assumptions first. In joint transmission CoMP (JTCoMP), the macrocell BS receives the data packets intended to a particular UE in the expanded region (ER) from the serving gateway (S-GW), then it designs the precoding vectors to be forwarded through a wired or wireless backhaul infrastructure to the other BSs in the cooperating cluster. Another option would be to send raw data along with the CSI to the microcell BSs, and to allow them to perform the precoding. In wired environments, the types of delay that would be of greatest concern are the transmission and propagation delay. In wireless environments, on the other hand, there is an additional access delay due to the possibility of having low SINR, which forces retransmissions. There are two wireless backhaul scenarios, with either shared or dedicated resources. With shared resources, the backhaul network would be communicating using the same time and frequency resources assigned to the UEs, which

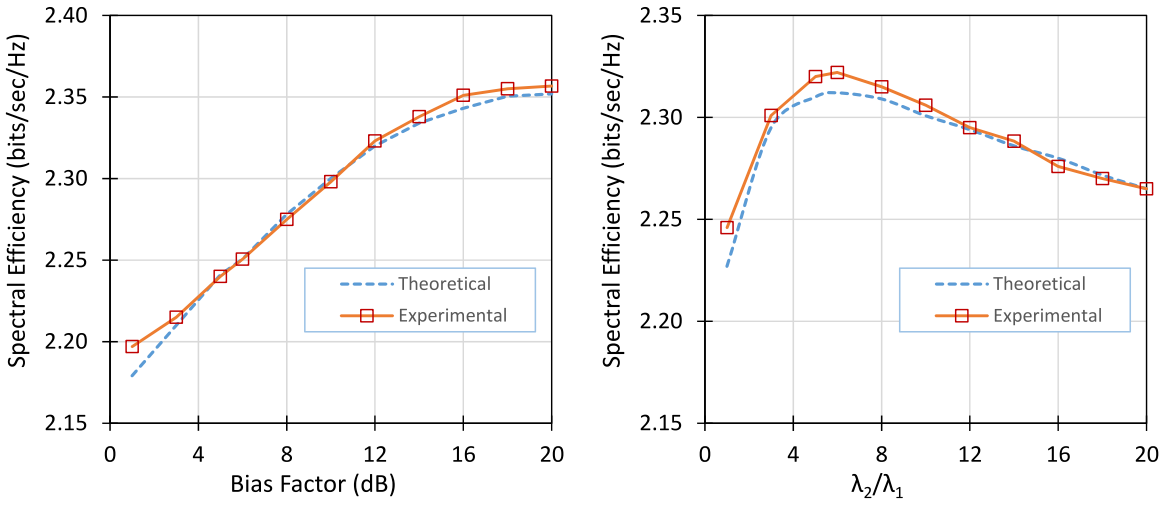

Fig. 7. Overall spectral efficiency for mode 2C only vs. β (left) and λ_2/λ_1 (right).

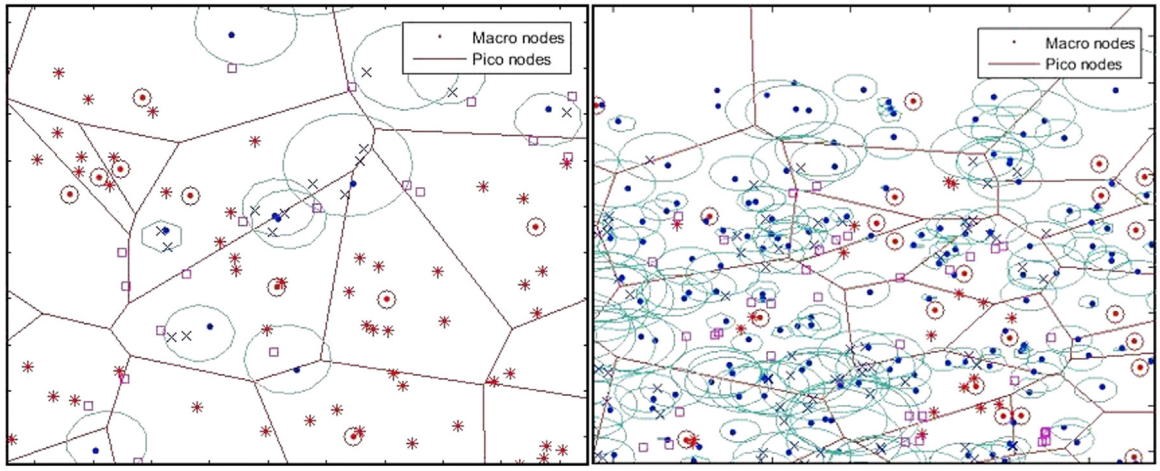

Fig. 8. BS and UE positions for two scenarios: $\lambda_2 = \lambda_1$(left) and $\lambda_2 = 8\lambda_1$ (right). Microcell BSs are the blue dots while macrocell BSs are the red circles with a dot in the center. Stars are UEs associated with the macrocell alone, while Xs are UEs associated with the microcell alone, and square UEs are in CoMP mode. The large circles represent the points where the power received from the macrocell becomes equal to the power received from the microcell. (For interpretation of the references to color in this figure legend, the reader is referred to the web version of this article.)

increases interference. However, dedicated resources mean that the backhaul transmissions are out of band, using millimeter wave frequencies, for instance, and do not interfere with UE transmission and reception.

6.1. Backhaul capacity

The use of JTCoMP leads to an increase in the volume of backhaul traffic, as a direct result of the need for a serving BS to send user data to other BSs in the cooperating set for joint transmission to the UE. To get an estimate of the capacity needed for a user, the spectral efficiency must be computed. This is measured in bits/sec/Hz and indicates the rate that can be provided for a given bandwidth. The expression for the overall spectral efficiency for users in each mode of operation is defined in (39) below, as in [5], and expanded as follows.

$$\begin{aligned} SE_i &= E_r\left[E_{SINR}\left[\log_2\left(1+SINR(B)\right)\right]\right] \\ &= \int_A E_{SINR}\left[\log_2\left(1+SINR(B)\right)\right] f_{R_i}(r)dr \\ &= \int_{R+}\left[\int_A P\left[\log_2\left(1+SINR(B)\right) > t\right] f_{R_i}(r)dr\right]dt \\ &= \int_{R+}\left[\int_A P\left[SINR(B) > 2^t - 1\right] f_{R_i}(r)dr\right]dt \end{aligned} \tag{39}$$

From the definition of outage probability in (16), we reduce the expression in (39) to

$$SE_i = \int_{R+} 1 - [O_i]_{\tau=2^t-1}dt. \tag{40}$$

where B is the UE's mode of operation, A is the area of integration based on user location in each mode of operation, O denotes the outage probability expression obtained in (17)–(20), and i indexes the spectral efficiencies, distance probability density functions, and outage probabilities for the different modes. Finally, the overall spectral efficiency can be expressed in (41), where q_M, q_P, q_{2C}, and q_{3C} are the probabilities of being in M, P, $2C$, and $3C$ respectively.

$$SE = q_M SE_M + q_P SE_P + q_{2C} SE_{2C} + q_{3C} SE_{3C} \tag{41}$$

Theoretical and experimental simulation spectral efficiency results are next analyzed for the different scenarios. In the first one, analytical results are shown for varying the threshold for the microcell ER (β) from zero to 20 dB, with CoMP in the microcell ER alone (Mode 2C only). This was based on (41), while setting q_M, q_P, and q_{3C} to 0, and setting q_{2C} to 1. The experimental results are also

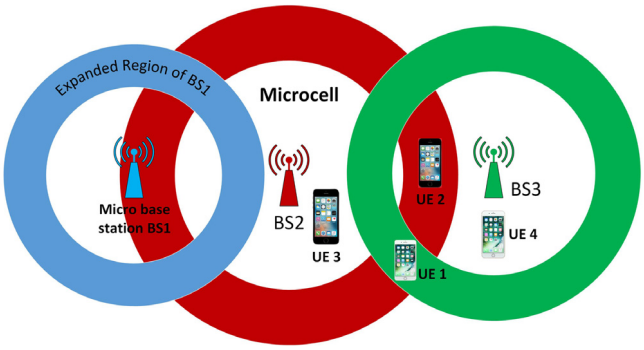

Fig. 9. Representation of closely located microcells.

plotted with the theoretical to show the latter's validity. The left graph of Fig. 7 shows the trend of the increase in the overall spectral efficiency, where it is seen how the experimental and analytical results overlap, thus rendering further validity to the analysis. To provide more insight, we vary the microcell BS intensity in the right graph of Fig. 7, which shows how the spectral increases until it peaks at $\lambda_2/\lambda_1 = 6$, i.e., when there are 6 times as many microcells as macrocells. As λ_2/λ_1 continues to rise, the spectral efficiency starts to drop due to the increase in interference from additional microcells operating within the transmission range of the macrocell.

Fig. 8 shows as the number of microcell BSs increases, the overlaps between them increases. This can be explained better using Fig. 9, which illustrates that as the number of microcells becomes too high, there would actually be fewer UEs that benefit from CoMP mode. This can be clarified by examining UE2, which would be served by only one microcell BS since it lies within the region where the power received from the microcell is stronger than that of the macrocell. However, UE2 would suffer from increased interference due to having many BSs close to each other. On the other hand, UE1 would be able to benefit from CoMP mode and UE3 would receive a stronger signal from its serving BS. As the number of microcells increases, the number of UEs that are like UE2 will increase as interference continues to rise. This explains the intuition behind having an optimal value for λ_2/λ_1 and for an ER threshold β. The spectral efficiency analyzed above will be used to derive the percentage increase in the backhaul capacity due to CoMP.

In order to view the consequence of CoMP on spectral efficiency in different scenarios, specifically modes 2C, 3C, and 5C, Fig. 10 is shown next. The numerical and analytical results in the figure (corresponding to (41)) show that there is a direct relation between the spectral efficiency and the maximum number of BSs in the CoMP cluster. As the number of such BSs changes from 2 to 3 to 5, we see how the spectral efficiency starts to increase as a direct result of having more users in CoMP mode, thus leading to higher overall SINR.

As described in [19] the amount of X2 backhaul traffic can be estimated as a percentage of the traffic of the S1 interface between the mobility management entity (MME) and the serving gateway (S-GW). As per [19], the amount of X2 traffic that accounts for handover is 4%, while the amount of traffic that takes into account transport protocol overhead is 10%. Based on these numbers and the analysis done in [20], we can state the amount of traffic passing through the backhaul as

$$C = 1.14BW(SE_i + SE_{CoMP}), \tag{42}$$

$$\text{where } SE_{CoMP} = \sum_{i \neq BS \text{ of int erest}} SE_i. \tag{43}$$

where BW is the bandwidth, SE_i is the spectral efficiency of each BS, and SE_{CoMP} is the spectral efficiency taking into account the data rates from other cooperating BSs, as seen in (43). The simulation and analytical results derived from (42) are shown in Fig. 11. In considering the left graph, we observe that as the value of β increases, we have more users participating in CoMP mode, and the amount of backhaul traffic increases up to 20% for 3C mode, and up to 30% for 5C. On the other hand, as illustrated in the right graph, when the number of microcells increases for a fixed value of β, the backhaul traffic increases up to a certain point (10% for 3C and 20% for 5C). This can be explained using the earlier analysis. Since the increase in the amount of microcell BSs beyond a certain point causes significant interference, the overall SINR in the network decreases, and this would lower the achievable rate.

6.2. Effect on backhaul delay

For the study of delay in our proposed system, we use the same infrastructure as described previously. The most significant delays to be discussed in relation to our system are the wireless access delays (i.e., between UE and BS) and the delays in the wired or wireless backhaul itself [21]. We first consider the effect of

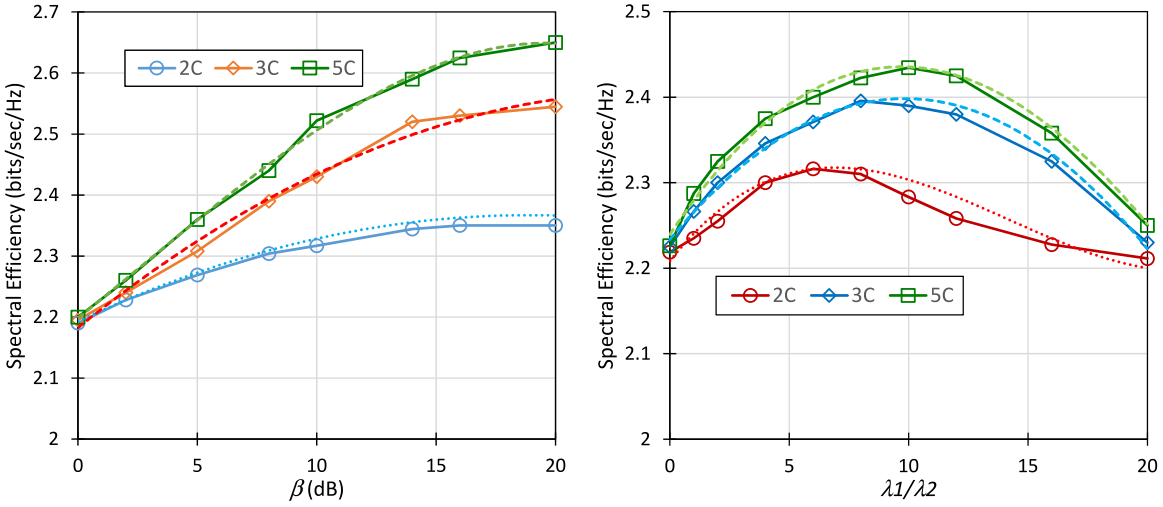

Fig. 10. Overall spectral efficiency vs. β (left), and vs. λ_2/λ_1 (right) with β set to 10 dB.

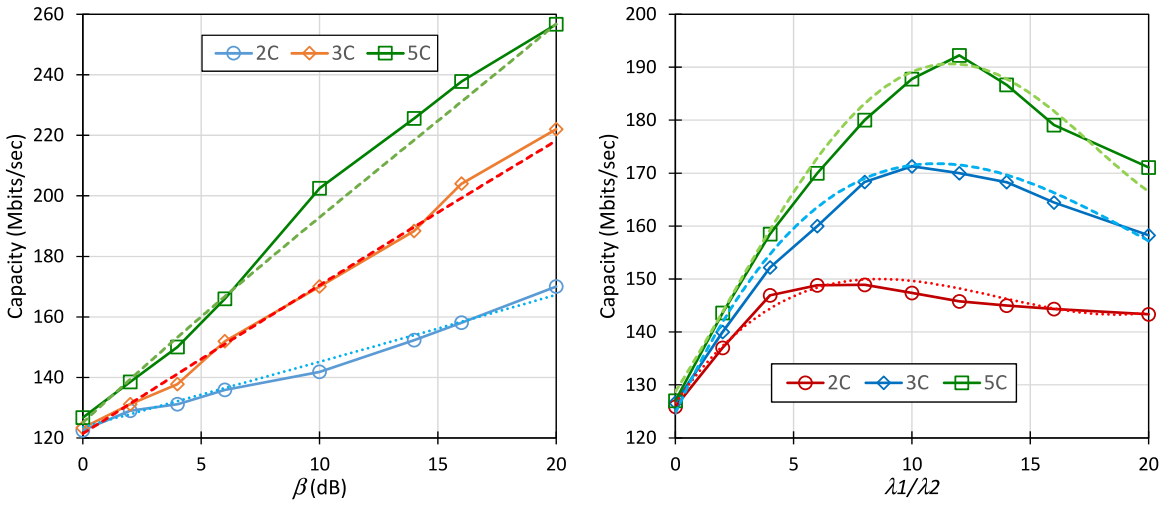

Fig. 11. Capacity vs. β (left) and vs. λ_2/λ_1 (right).

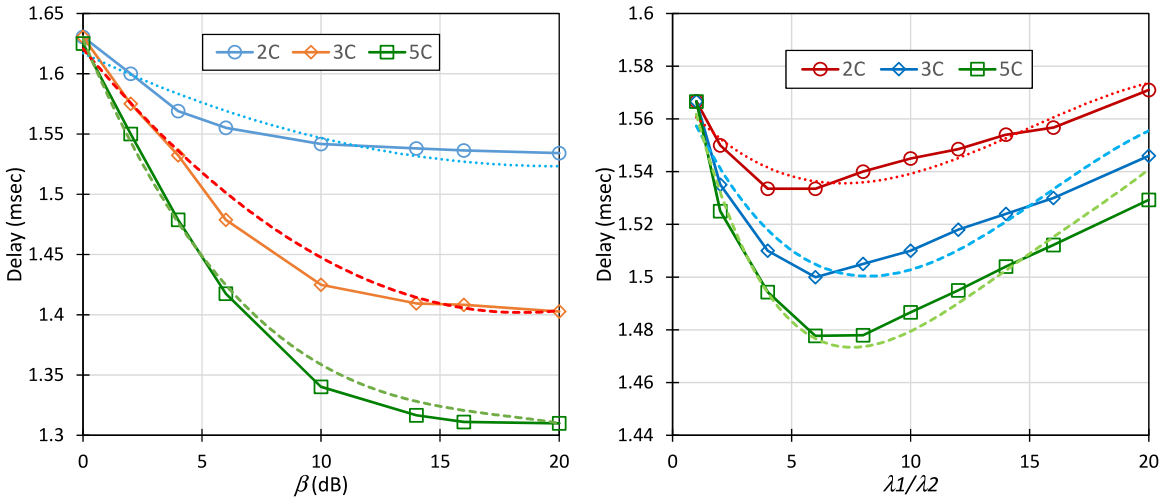

Fig. 12. UE wireless access delay vs. β (left), and vs. λ_2/λ_1 with $\beta = 10$ dB (right).

the wireless access delay, which, as discussed in [21], is due to retransmissions from failed data packets, which are allowed to occur up to M times, after which there is a failed transmission. A packet needs to be retransmitted whenever the SINR at a UE is below a certain threshold, meaning that we can use the outage probabilities of (38) to obtain the average overall wireless access delay. If T_1 is the time taken for a single transmission from the BS to the UE, then the expected delay is greater than or equal to T_1 with a probability equals to 1, and the probability of a failure to occur one time is the outage probability itself, which results in a delay that is equal to twice T_1. The probability of a third failure is the outage probability squared and requires an added delay of T_1 as well [21]. Therefore, the expected UE access delay is as follows.

$$E[D] = T_1\left[1 + O + O^2 + \cdots + O^{M-1}\right] = \frac{T_1\left(1 - O^M\right)}{1 - O} \tag{44}$$

In Fig. 12, numerical and theoretical results (based on (44) above, and the outage probabilities in (38)) are provided for the average delay due to outage probability. The value of T_1 was set to 1 and the simulation was run over values of microcell BS intensity varying from $\lambda_2 = (500\times 2\pi)^{-1}$ to 20 times that, while the macrocell BS intensity was fixed at $\lambda_1 = (500\times 2\pi)^{-1}$. At the same time, results are shown for fixing the microcell BS intensity at $10\times(500\times 2\pi)^{-1}$ and varying the ER threshold β from 0 to 20 dBs. As can be seen in the figure, the delay due to wireless retransmissions from the BSs to the UEs depends on both β and the number of macrocell BSs in the network. As the value of β increases, the outage probability decreases and so does the overall number of retransmissions. However, when the number of microcell BSs continues to rise, we only benefit up to a certain point, which is around 8 microcells to every macrocell (in the case of 5C). Further increases in the number of microcell BSs would lead to higher delay values.

The above results also illustrate how our proposed scheme that treats cooperation in overlap regions differently increases the ratio of allowable microcells per macrocell (e.g., from 4, to 6, to 8, going from 2C to 3C to 5C, as depicted in the right graph), and thus serves to increase the scalability of the network. Hence, the result can be used by network operators as a factor when making microcell deployment decisions to keep the delay in the backhaul below a certain threshold.

In the next subsection, we study the effect of adding backhaul delay to the access delay obtained above. The delay depends on the used technology, and so, we consider wired backhaul delay, wireless backhaul delay with dedicated resources, and wireless backhaul delay with shared resources.

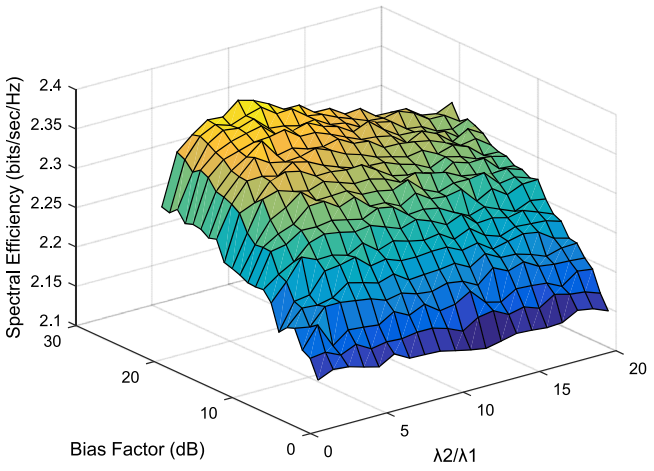

Fig. 13. Spectral efficiency vs. β and λ_2/λ_1.

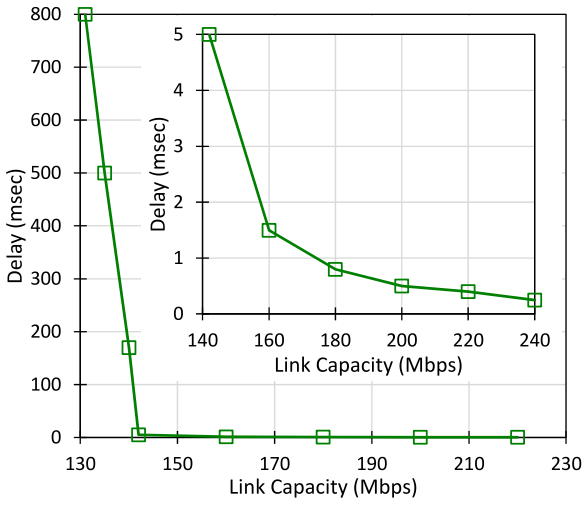

Fig. 14. Wired backhaul delay vs. link capacity for $\lambda_2 = 6\lambda_1$ and $\beta = 20$ dB.

6.2.1. Delay for wired backhaul links

The wired backhaul can be modeled as a queue [22], and the delay is obtained using Littles Law.

$$D = \frac{\lambda_{traffic}}{2\mu_{cap}\left(\mu_{cap} - \lambda_{traffic}\right)} \tag{45}$$

where $\lambda_{traffic}$ is the amount of traffic on the backhaul links, and μ_{cap} is the backhaul link capacity. The delay value depends on the link capacity which we vary based on the results obtained in the surface plot shown in Fig. 13. The results illustrate that we have the highest spectral efficiency when β is 20 dB and λ_2 is at $8\lambda_1$. This is because the overall SINR becomes lower as β increases due to having more UEs in CoMP mode. It also appears that there is an optimal value at the peak of the surface plot for the number of microcell BSs with respect to the number of macrocell BSs. This means that beyond a certain value, the increase in λ_2 leads to a rise in the amount of interference experienced by the UE as can be experienced by a lower overall spectral efficiency.

Based on the results in Fig. 13, we consider a value of β equal to 20 dB and a value of λ_2 equal to $6\lambda_1$, thus corresponding to 132 Mbps of traffic volume that is traveling through the backhaul links. This value is obtained through simulations based on the relation between capacity and spectral efficiency. In order to have a stable system, the backhaul link capacity must be greater than the amount of traffic on the backhaul. By fixing the traffic volume to 132 Mbps, we therefore vary the capacity of the backhaul links from 132 to 240 Mbps to study the resulting delay (corresponding to (45)), which we show in Fig. 14.

6.2.2. Delay for wireless backhaul links with shared resources

In the case of wireless links with shared resources, the wireless communication resulting from the X2 interface would interfere with other network transmissions. The microcell can be considered to have the same outage probability as a UE that is associated with its macrocell, with probability equal to 1. This way, we can set $q_M = 1$ and $q_C = q_P = 0$.

$$f_{R_{shared}}(r) = 2\pi\lambda_1 r \exp\left[-\pi\left(\lambda_1 r^2 + \lambda_2\left(\frac{\beta P_2}{P_1}\right)^{\frac{2}{\alpha_2}} r^{\frac{2\alpha 1}{\alpha_2}}\right)\right] \tag{46}$$

Here, the microcell BS is always receiving user data from the macrocell BS, and hence, the resulting outage probability is similar to the one experienced by UEs connecting to the macrocell BS.

$$O_{b\text{-}shared} = 1 - \int_{R+} \exp\left[\frac{-\theta\sigma_z^2}{P_1 r^{-\alpha_1}}\right] \prod_{j=1}^{2} L_{l_j}\left(\frac{\theta r^{\alpha_1}}{P_1}\right) f_{R_{shared}}(r)\, dr \tag{47}$$

6.2.3. Delay for wireless backhaul links with dedicated resources

Finally, the outage probability in case of dedicated resources can be treated as in [21], where the wireless backhaul is assumed not to interfere with the transmissions intended for UEs. In this case, we need to consider the probability density function of the distance between two successive tiers in a Poisson Point Process. This is shown as follows.

$$f_{R_{dedicated}}(r) = 2\pi\lambda_1 r \exp\left[-\pi\lambda_1 r^2\right] \tag{48}$$

$$O_{b\text{-}dedicated} = 1 - \int_{R+} \exp\left[\frac{-\theta\sigma_z^2}{P_1 r^{-\alpha_1}}\right] \prod_{j=1}^{2} L_{l_j}\left(\frac{\theta r^{\alpha_1}}{P_1}\right) f_{R_{dedicated}}(r)\, dr \tag{49}$$

Fig. 15 illustrates the numerical delay results of all three backhaul technologies. We point out that the delays for wired backhaul links correspond to (45), the delays for wireless backhaul links with shared resources correspond to (44) and using the outage probability in (47), and finally, the delays for wireless backhaul links with dedicated resources also correspond to (44), but incorporate (49). As can be seen in the figure, the backhaul delay varies from one technology to another. For instance, the wireless backhaul delay tells us that there is an optimal value for the microcell BS intensity, beyond which performance begins to degrade. At the same time, we observe that the delay for the wired backhaul starts to decrease beyond $6\lambda_2/\lambda_1$. This means that the number of microcell BSs can be increased at the expense of having lower overall SINR. Furthermore, as the bias factor increases, we see a rise in the delay as well, except in the dedicated resources case. This can be explained by the fact that as the bias factor starts to increase, we would have more microcell BSs cooperating with the macrocell. This in turn implies that transmissions from macrocells to nearby microcells would no longer interfere with each other, nor with regular network traffic.

7. Conclusion

In this paper, we have analyzed the outage probability of a two-tier cellular network while considering the effect of overlaps in the microcell expanded regions, and thus took into account network environments that are characterized with dense microcell deployments. Our scheme allows for better mitigation of co-tier interference within a HetNet since microcells located in densely populated areas might be in close proximity to each other, and

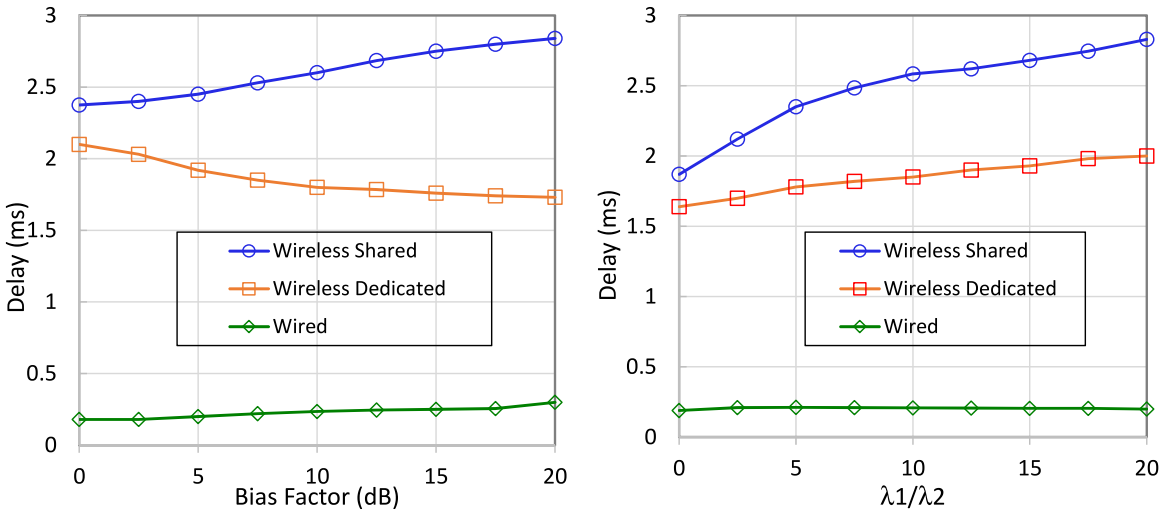

Fig. 15. Overall (UE access + backhaul) delay vs. β (left) and λ_2/λ_1 (right).

it thus offers a more scalable framework that can be applicable to more scenarios. We also focused on the implications of our CoMP scheme on the different backhaul architectures, and more specifically, we analyzed the effect on the capacity of backhaul links and on the UE overall communication delay, and came up with conclusions regarding microcell deployment scenarios.

Acknowledgment

The authors would like to acknowledge the generous support of the University Research Board (URB) of the American University of Beirut, Project no. 24115.

References

[1] Akyildiz, D.M. Gutierrez-Estevez, R. Balakrishnan, E. Chavarria Reyes, LTE-advanced and the evolution to beyond 4G (B4G) systems, in: Physical Communications, vol. 10, Mar. 2014, pp. 31–60.
[2] W. Zirwas, U. Zeeshan, M. Grieger, Cooperative feeder links for relay enhanced networks, in: 18th European Wireless Conference, April 2012, pp. 1–8.
[3] D. Lopez-Perez, X. Chu, I. Guvenc, On the expanded Region of Picocells in Heterogeneous Networks, IEEE J. Sel. Top. Sign. Proces. 6 (3) (2012) 281–294.
[4] T. Saouma, H. Artail, Y. Nasser, Involving already deployed RNs in joint processing coordinated multipoint, in: Sixth International Conference on Digital Information Processing and Communications, ICDIPC 2016, Beirut, Lebanon, April 2016.
[5] A. Sakr, E. Hossain, Location-aware cross-tier coordinated multipoint transmission in two-tier cellular networks, IEEE Trans. Wirel. Commun. 13 (11) (2014) 6311–6325.
[6] J. Khoriaty, H. Artail, Coordinated multipoint in heterogeneous networks with overlapping microcell expanded regions, in: 2015 IEEE 11th International Conference on Wireless and Mobile Computing, Networking and Communications, WiMob, Abu Dhabi, 2015, pp. 289–295.
[7] H. Dhillon, R. Ganti, F. Baccelli, J. Andrews, Modeling and analysis of k-tier downlink heterogeneous cellular networks, IEEE J. Sel. Areas Commun. 30 (3) (2012) 550–560.
[8] S. Kshatriya, S. Kaimalettu, S. Yerrapareddy, K. Milleth, N. Akhtar, On interference management based on subframe blanking in Heterogeneous LTE networks, in: Fifth International Conference on Communication Systems and Networks, COMSNETS, Jan 2013, pp. 1–7.
[9] D. Lee, H. Seo, B. Clerckx, E. Hardouin, D. Mazzarese, S. Nagata, K. Sayana, Coordinated multipoint transmission and reception in LTE-advanced: deployment scenarios and operational challenges, IEEE Commun. Mag. 50 (2) (2012) 148–155.
[10] G. Nigam, P. Minero, M. Haenggi, Coordinated multipoint joint transmission in heterogeneous networks, IEEE Trans. Commun. 62 (11) (2014) 4134–4146.
[11] F. Boccardi, H. Huang, A. Alexiou, Network MIMO with reduced backhaul requirements by MAC coordination, in: 42nd Asilomar Conference on Signals, Systems and Computers, Oct. 2008, pp. 1125–1129.
[12] P. Marsch, G. Fettweis, A framework for optimizing the uplink performance of distributed antenna systems under a constrained backhaul, in: IEEE International Conference on Communications, ICC '07, June 2007, pp. 975–979.
[13] P. Marsch, G. Fettweis, A decentralized optimization approach to backhaul-constrained distributed antenna systems, in: 16th IST Mobile and Wireless Communications Summit, July 2007, pp. 1–5.
[14] P. Marsch, G. Fettweis, On base station cooperation schemes for downlink network MIMO under a constrained backhaul, in: 2008. IEEE Global Telecommunications Conference, GLOBECOM, Dec. 4 2008, pp. 1–6.
[15] T. Biermann, L. Scalia, C. Changsoon, W. Kellerer, H. Karl, How backhaul networks influence the feasibility of coordinated multipoint in cellular networks, IEEE Commun. Mag. 51 (8) (2013) 168–176.
[16] Z. Mayer, L. Jingya, A. Papadogiannis, T. Svensson, On the impact of backhaul channel reliability on cooperative wireless networks, in: 2013 IEEE International Conference on Communications, ICC, June 2013, pp. 5284–5289.
[17] V. Jungnickel, S. Jaeckel, K. Borner, M. Schlosser, L. Thiele, Estimating the mobile backhaul traffic in distributed coordinated multi-point systems, in: IEEE Wireless Communications and Networking Conference, WCNC, April 2012, pp. 3763–3768.
[18] D. Samardzija, H. Huang, Determining backhaul bandwidth requirements for network MIMO, in: 17th European in Signal Processing Conference, Aug. 2009, pp. 1494–1498.
[19] J. Robson, Guidelines for LTE Backhaul Traffic Estimation, in: NGMN White Paper, Jul. 2011, pp. 1–18.
[20] V. Jungnickel, K. Manolakis, S. Jaeckel, M. Lossow, P. Farkas, M. Schlosser, V. and Braun, Backhaul requirements for inter-site cooperation in heterogeneous LTE-Advanced networks, in: IEEE International Conference on Communications, ICC, June 2013, pp. 905–910.
[21] D. Chen, T. Quek, M. Kountouris, Backhauling in heterogeneous cellular networks: Modeling and tradeoffs, IEEE Trans. Wirel. Commun. 14 (6) (2015) 3194–3206.
[22] F. Pantisano, M. Bennis, W. Saad, M. Debbah, M. Latva-aho, On the impact of heterogeneous backhauls on coordinated multipoint transmission in femtocell networks, in: IEEE International Conference on Communications, ICC, Ottawa, ON, 2012, pp. 5064–5069.

Jessica Khoriaty completed the Bachelor in Engineering (BE) degree in Computer and Communications Engineering (CCE) with distinction in 2014 from the American University of Beirut (AUB), and the Master in Engineering in 2016. Jessikas research interests are in wireless communication and cooperative networks. She is currently a Ph.D. student at the University of Waterloo.

Hassan Artail is a Professor in the Department of Electrical and Computer Engineering at the American University of Beirut (AUB), doing research in the areas of mobile computing, vehicle ad hoc networks, 5G, and Internet of Things. Prior to joining AUB, Dr. Artail was a system development supervisor at the Scientific Labs of Daimler-Chrysler, Michigan where he worked for 11 years in the field of software and system development for vehicle testing applications. He obtained a B.S. with high distinction and an M.S. in Electrical and Computer Engineering from the University of Detroit in 1985 and 1986 respectively, and a Ph.D. from Wayne State University in 1999. Since joining AUB, Dr. Artail published over 200 articles in reputable journals and top conferences. He obtained several awards, including the Research Excellence Award from the Lebanese National Council for Scientific Research, for contributions in the area of Information & Communication Technology in July 2012, and the Career Excellence in Scientific Research Award from the Lebanese Association for the Advancement of Science (LAAS) in April 2017.

Youssef Nasser obtained his Masters and Ph.D. degrees in Signal Processing and Communications from the National Polytechnic Institute of Grenoble, France in 2003 and 2006 respectively and his 'Habilitation à Diriger la Recherche (HDR), diploma, the highest education degree a scholar can achieve, in 2015. He is currently with the Department of Electrical and Computer Engineering at the American University of Beirut. From 2006 to 2010, he worked as a Senior Research Engineer with the Institute of Electronics and Telecommunications of Rennes (IETR), France. From 2003 to 2006, he worked with the Laboratory of Electronics and Information Technologies in Grenoble (Laboratoire d'Electronique et de Technologies de l'Information — LETI) as a R&D Engineer. Since 2007, Y. Nasser is involved in the standardization of European broadcasting systems including DVB-T2, DVB-T2 Lite and DVB-NGH. He coordinated tasks and/or packages of many European projects. Y. Nasser has published more than 100 papers in international peer-reviewed journals and conferences. Since 2011 He is a Senior Member of the IEEE.